

Electrical Signature of Brine Percolation in Sea Ice

Kenneth M. Golden^{*}, Hajo Eicken[†], Adam Gully^{*}, Malcolm Ingham[‡], Keleigh A. Jones[‡], Joyce Lin^{*}, James E. Reid[§], Christian S. Sampson^{*}, and Anthony P. Worby[¶]

^{*}Department of Mathematics, University of Utah, USA, [†]University of Alaska Fairbanks, USA, [‡]School of Chemical and Physical Sciences, Victoria University of Wellington, NZ, [§]Groundprobe Geophysics, Malaga, AU, and [¶]Australian Antarctic Division and ACE CRC, University of Tasmania, AU

Submitted to Proceedings of the National Academy of Sciences of the United States of America

Fluid flow through sea ice mediates a broad range of geophysical and biological processes in the polar marine environment. For example, the evolution of melt ponds and sea ice albedo, which is important in climate modeling, is constrained by drainage through the porous brine microstructure. Fluid flow also facilitates snow-ice formation, the evolution of the salt budget, and biomass build-up sustained by nutrient fluxes. However, for brine volume fractions below about 5%, columnar sea ice is effectively impermeable to fluid flow, which controls these processes. In two different experiments conducted in the Arctic and Antarctic, we have found that this critical transition in fluid flow exhibits a strong electrical signature, with sea ice resistivity sharply rising over three orders of magnitude near the brine connectivity threshold. The data are accurately explained by percolation theory, with the same universal critical exponent of 2 which captures the behavior of the fluid permeability. Our results demonstrate that classical lattice models of phase transitions in statistical physics can help unravel the complexity of transport in this multi-scale random medium. The theory enables electrical classification of sea ice layers in terms of their fluid flow properties, thus connecting specific electrical signatures to important transport processes such as melt pond drainage, CO₂ pumping, and nutrient fluxes. Our findings lay the foundation for electromagnetic monitoring of transport phenomena in sea ice, which can help track key transitions in the state of polar sea ice and improve projections of its fate and impact on ecosystems.

sea ice | percolation | fluid transport | electrical transport

Introduction

Polar sea ice is a key component of Earth's climate system, and a leading indicator of climate change [1, 2, 3]. As a material sea ice is a composite of pure ice with brine and air inclusions. The brine microstructure hosts extensive algal and bacterial communities which sustain life in the polar oceans [1, 4, 5, 6, 7]. While global climate models predict declines in sea ice area and thickness, they have significantly underestimated the recent loss in Arctic summer ice extent [3]. We focus here on sea ice transport processes which are critical to the role that sea ice plays in climate, and can lead to more realistic representations of sea ice in climate models. In particular, we investigate the electrical behavior of sea ice associated with fluid transport phenomena and microstructural transitions.

Improving projections of the fate of Earth's sea ice cover and its ecosystems depends on a better understanding of important processes and feedback mechanisms. During the melt season the Arctic sea ice cover becomes a complex, evolving mosaic of ice, melt ponds, and open water. While snow and ice reflect most incident sunlight, melt ponds and ocean absorb most of it. The reflectance or albedo of sea ice floes is determined by melt pond evolution [8, 9, 10]. Drainage of the ponds, with a resulting increase in albedo, is largely controlled by the fluid permeability of the porous sea ice underlying the ponds [11, 12]. As ice recedes with melting, more water surface is exposed, which increases solar absorption, leading in turn to more melting, and so on. This *ice-albedo feedback* has played a significant role in the decline of the summer Arctic ice pack [13, 14]. Moreover, it is the driving mechanism in math-

ematical models of whether we have passed a *tipping point* or *critical threshold* in the decline of summer Arctic sea ice [15, 16]. Sea ice albedo also represents a significant source of uncertainty in climate projections and a fundamental problem in climate modeling [17, 9, 18, 10].

Fluid flow through sea ice also governs the evolution of the salt budget and salinity profiles [1], convection-enhanced thermal transport [19], ocean-ice-atmosphere CO₂ exchanges [20], and the build-up of algal biomass fueled by fluxes of nutrients [1, 4]. It also drives snow-ice formation, which accounts for a significant portion of the ice produced in the Southern Ocean [21]. Sea water percolates upward through the porous brine microstructure, flooding the snow layer, which subsequently freezes.

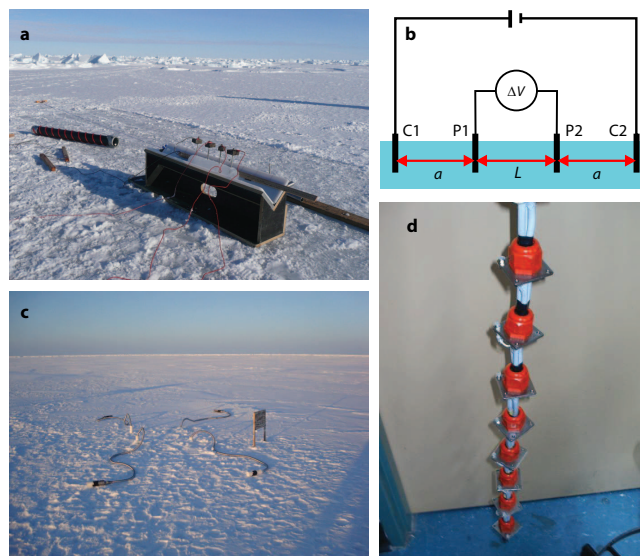


Fig. 1. (a) A Wenner electrode array is configured to measure the vertical conductivity of Antarctic sea ice, by inserting the four probes into an extracted ice core. (b) A current I is injected into the core through the outer electrodes C1 and C2. The potential difference ΔV resulting from the current flow is measured by the inner electrodes P1 and P2. The ratio $\Delta V/I$ is the resistance R in ohms. Here the electrode spacing is $L = 10$ cm and $a = 10$ cm. (c) A cross-borehole array is frozen into Arctic sea ice. The DC resistivity profile was tomographically reconstructed in the volume enclosed by the electrode strings. One of the strings, with 10 cm separation of the plates, is shown in (d).

Reserved for Publication Footnotes

While fluid flow is substantially restricted for brine volume fractions ϕ below about 5%, columnar sea ice is increasingly permeable for ϕ above 5% [22]. For a typical bulk salinity of 5 ppt, the critical porosity $\phi_c \approx 5\%$ corresponds to a temperature $T_c \approx -5^\circ\text{C}$, which is known as the *rule of fives*. This critical behavior of the fluid permeability results from a connectivity or percolation threshold in the brine microstructure [22, 12, 23]. If the fluid transport properties of sea ice can be linked to its electrical properties, which is the aim of this paper, then new approaches can be brought to bear in monitoring the state of sea ice. For example, it could open the door to the development of sensors to enhance existing buoy networks, provide information on key ice processes, and improve integration with satellite data.

The electrical conductivity of sea ice has been studied over the past five decades [24, 25, 26, 27, 28, 29]. However, there have been no observations of critical behavior in electrical properties corresponding to the microstructural transition encapsulated in the rule of fives. Here we report on two types of experiments where electrical resistivity data clearly display critical behavior at the brine percolation threshold. The mathematical description we develop provides a rigorous link between fluid and electrical transport in sea ice, with both displaying the same type of universal critical behavior, thus laying the foundation for the techniques referred to above. In fact, we further develop this foundation by partitioning the range of resistivity values of our data into intervals which correspond to distinct regimes of fluid permeability characteristics and related process behavior, such as melt pond development, and fluxes of nutrients and CO_2 .

One of the goals of this work is to obtain data on the linkages between electrical and hydraulic properties, yielding information about key microstructural variables in the process [30]. The value of such an approach lies in the potential to then extract information about other key variables describing the state of sea ice, e.g., pertaining to its rheology or potential to harbor microbial communities, from measurements of electric properties which are more easily obtained, e.g., from *in situ* drifting sensors that can monitor the evolution of sea ice non-destructively (Figure 1 d).

The findings presented here also have implications for measuring ice thickness, an important gauge of the impact of global warming. Not only is thickness data important in comparing climate model predictions to observed behavior, but in specifying the initial conditions necessary for long-term numerical simulations. Promising techniques for advanced airborne or surface-based measurements of ice thickness depend on the interaction of electromagnetic (EM) fields with sea ice. For example, there has been significant interest in the development of EM induction devices [31, 28] mounted on ships, planes and helicopters. These techniques, and the interpretation of the data to obtain thickness information, rely on knowledge of the electrical properties of sea ice, and how they vary with depth, temperature, salinity, and ice type. The results presented here shed significant light on such issues.

Results

Sea ice is an anisotropic composite with vertically elongated brine inclusions and corresponding anisotropy in the effective fluid permeability and electrical conductivity tensors. Most methods for measuring sea ice conductivity involve indirect or inverse techniques, such as surface-based geoelectric profiling using a Wenner array of electrodes [24, 26, 27, 28, 29, 32]. Generally with these methods the vertical conductivity σ_v^* is

inherently mixed with the horizontal components. Here we are most interested in σ_v^* due to its connection with vertical fluid flow.

During the Sea Ice Physics and Ecosystem Experiment (SIPEX) in September and October of 2007, we made *direct* measurements of σ_v^* in Antarctic pack ice by adapting a four probe Wenner array for use in cylindrical ice cores, as shown in Figure 1 a and b. The study area was located off the coast of East Antarctica, between 115°E and 130°E , and 64°S and 66°S . At 8 of the 15 ice stations along the cruise track of the Australian icebreaker *Aurora Australis*, we extracted vertical cores from thin first-year sea ice, with lengths ranging from 34 cm to 86 cm. We obtained 26 averaged data points from 67 raw measurements of the resistance between the inner probes. We also measured temperature and salinity profiles for the cores, so that the data on σ_v^* could be viewed as a function of brine volume fraction ϕ (see Methods).

In the Arctic, we used the technique of cross-borehole DC resistivity tomography [29, 33], as shown in Figure 1 c and d. The ice is probed in its natural state, utilizing two or four vertical strings of electrodes frozen into the ice. It has been shown that this method can be used to derive the horizontal component of the anisotropic resistivity profile. Moreover, it has recently been demonstrated that the vertical component

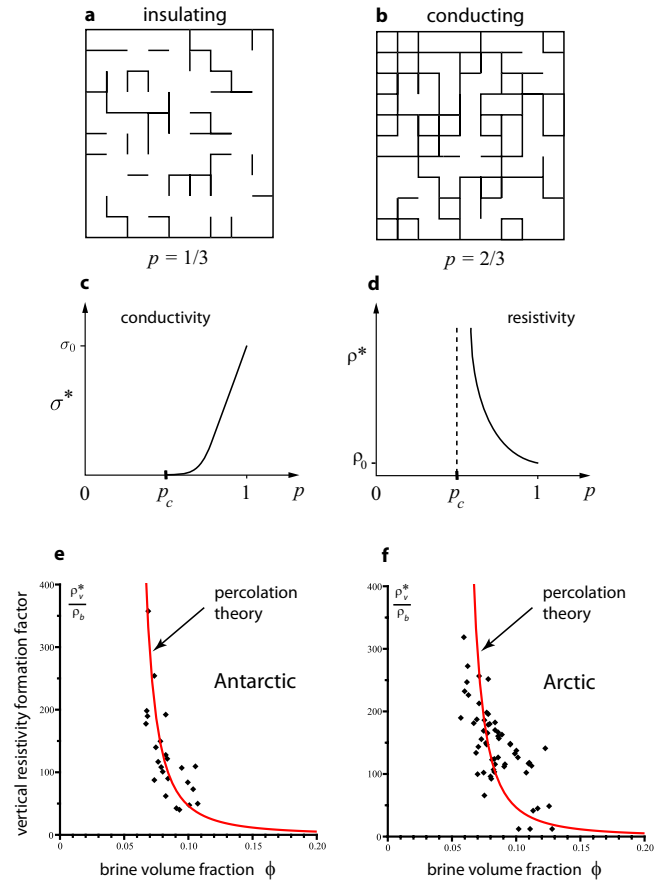


Fig. 2. The two dimensional square bond lattice below its percolation or connectivity threshold $p_c = 1/2$ in (a), and above in (b). Below p_c , there is no bulk transport, and above p_c the effective conductivity takes off with power law behavior, as shown in (c). In (d) the effective resistivity diverges as p approaches p_c from the right, with a vertical asymptote at $p = p_c$. We display the vertical resistivity formation factor data from the Antarctic in (e) and the Arctic in (f), along with the same prediction from percolation theory in each. Both data and theory exhibit divergent behavior as ϕ approaches $\phi_c \approx 0.05$ from the right, with a vertical asymptote at $\phi = \phi_c$, electrically signaling the transition to relatively impermeable ice.

of σ^* can be obtained as well [33, 29]. If a minimum of four electrode strings are used, the geometric mean of the vertical and horizontal components of σ^* can be derived, along with the horizontal component [29], yielding the vertical component.

Measurements of the temporal variation in the resistivity structure of first-year Arctic sea ice through spring warming have been made approximately 1 km off the coast of Barrow, Alaska at $71^\circ 21' 56.45''$ N, $156^\circ 32' 39.01''$ W. Electrode strings were installed in landfast first year ice in late January 2008. Cross-borehole measurements were made on 6 separate occasions between early April and mid June 2008, allowing both the horizontal and vertical components of the ice resistivity to be derived. A sea ice mass balance site and an ice core sampling program at the same location [34] provided ice temperature and salinity data, allowing the variation in resistivity structure to be correlated with brine volume fraction ϕ .

Lattice and continuum percolation theories [35] have been used to model a broad range of disordered materials where the connectedness of one phase dominates effective transport behavior. Consider the square ($d = 2$) or cubic ($d = 3$) network of bonds joining nearest neighbor sites on the integer lattice \mathbb{Z}^d . The bonds are assigned electrical conductivities $\sigma_0 > 0$ (open) or 0 (closed) with probabilities p and $1 - p$. Groups of connected open bonds are called open clusters, and the average cluster size grows as p increases. In this model there is a critical probability p_c , $0 < p_c < 1$, called the *percolation threshold*, where an infinite cluster of open bonds first appears. In $d = 2$, $p_c = \frac{1}{2}$, and in $d = 3$, $p_c \approx 0.25$. Typical configurations for the $d = 2$ square lattice above and below the threshold are shown in Figure 2 a and b.

Let $\sigma^*(p)$ be the effective conductivity of the network in the vertical direction [35]. For $p < p_c$, $\sigma^*(p) = 0$, as shown in Figure 2 c. For $p > p_c$ and near p_c , $\sigma^*(p)$ exhibits power law behavior,

$$\sigma^*(p) \sim \sigma_0(p - p_c)^t, \quad p \rightarrow p_c^+, \quad [1]$$

where t is the conductivity critical exponent. For lattices, t is believed to be universal, depending only on d . In $d = 2$, $t \approx 1.3$, and in $d = 3$, $t \approx 2.0$ [35]. There is also a rigorous bound [36] that $1 \leq t \leq 2$ in $d = 2$ and $d = 3$. Since $\sigma^*(p) \rightarrow 0$ as $p \rightarrow p_c^+$, the effective resistivity $\rho^*(p) = 1/\sigma^*(p)$ diverges as $p \rightarrow p_c^+$, with a vertical asymptote at $p = p_c$, as shown in Figure 2 d. It should be remarked that for samples of two phase composites with finite component resistivities, like sea ice, the behavior only approximates the asymptote, and for $p < p_c$, ρ^* remains finite.

The fluid permeability $\kappa^*(p)$ corresponding to (1), where the open bonds are pipes of fluid conductivity $\kappa_0/\eta = r_0^2/8\eta$ and radius r_0 , behaves like $\kappa^*(p) \sim \kappa_0(p - p_c)^e$ as $p \rightarrow p_c^+$, with e the fluid permeability exponent and η the fluid viscosity. For lattices, it is believed [35] that $e = t$. In the continuum, the exponents e and t can take non-universal values, and need not be equal, such as for the three dimensional Swiss cheese model [37, 35]. However, for lognormally distributed inclusions, as in sea ice, the behavior is *universal* [12, 38]. Thus for sea ice, $t = e \approx 2$.

In order to use percolation theory to quantitatively describe the vertical conductivity $\sigma_v^*(\phi)$, and to provide a link between fluid and electrical transport in sea ice, we recall our result [12] for the vertical fluid permeability

$$k_v^*(\phi) \sim 3(\phi - \phi_c)^2 \times 10^{-8} \text{ m}^2, \quad \phi \rightarrow \phi_c^+. \quad [2]$$

The scaling factor $k_0 = 3 \times 10^{-8}$ is estimated using critical path analysis [35, 39]. The effective behavior of media with a broad range of local conductances is dominated by a criti-

cal *bottleneck* conductance related to the minimal radius in a connected pathway of appropriate scale. To relate σ_v^* to k_v^* , we use the following relation from critical path analysis [39]. With r_c denoting the critical radius for our centimeter scale electrical experiments, then

$$k_v^* = \frac{r_c^2}{8} \frac{\sigma_v^*}{\sigma_b}, \quad [3]$$

where σ_b is the conductivity of brine, which depends [40] on temperature T . By measuring the radii of vertical pathways

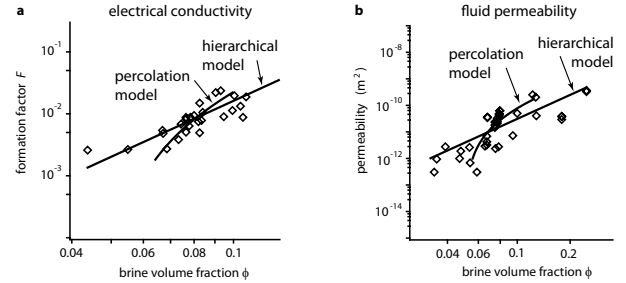


Fig. 3. (a) Antarctic field data on the vertical formation factor $F = \sigma_v^*/\sigma_b$ is compared with the hierarchical model $F(\phi) = F_0\phi^3$. The prediction of percolation theory is also shown. (b) Comparison of Arctic fluid permeability data with the hierarchical model, along with percolation theory [12]. In both figures percolation theory captures the trend of the data in the percolation regime more closely than Archie's law.

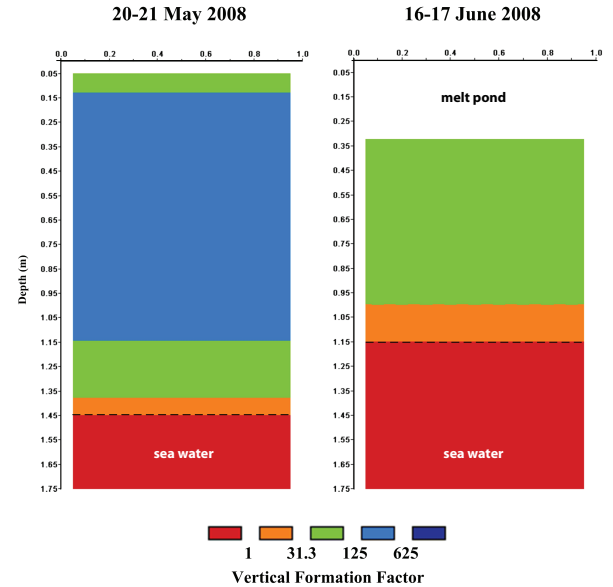


Fig. 4. Cross-borehole tomographic reconstructions of the vertical resistivity formation factor for Arctic sea ice before (a) and after (b) melt pond formation. The evolution of resistivity structure seen here is consistent with warming of the ice, thus increasing the fluid permeability and facilitating the infiltration of meltwater into the upper layer of sea ice from the surface. To help connect the electrical properties of sea ice to its important processes, the range of the resistivity formation factor G can be divided into five regimes: $G > 625$ (ice impermeable enough to allow ponds to grow for surface ablation rates 10 cm/d or larger for a critical pore radius of 0.1 mm); $125 < G \leq 625$, blue (ice impermeable enough to allow ponds to grow for surface ablation rates between 10 and 50 cm/d for a critical pore radius of 0.1 mm); $31.3 < G \leq 125$, green (at formation factors of 31.3 or larger ice is impermeable from the perspective of CO_2 exchange and build-up of nutrients and biomass in the ice [41], and sufficiently impermeable to fluid drainage to support surface ponding); $1 < G \leq 31.3$, orange (highly permeable ice that allows for CO_2 pumping and build-up of nutrients and biomass); $G \leq 1$, red (assumed to be free water column). Only the most resistive ice $G > 625$ is not shown in the figure.

in X-ray tomography images [12, 23], we estimate a range in mm of $0.1 \leq r_c \leq 0.2$.

It is useful to consider the vertical conductivity formation factor $F = \sigma_v^*/\sigma_b$, which removes the dependence of the effective parameter on the changing conductivity of the brine, and depends only on the pore volume fraction and geometry. In view of (1) and (3), $F(\phi) \sim F_0 (\phi - \phi_c)^2$ as $\phi \rightarrow \phi_c^+$, where $F_0 = 8k_0/r_c^2$. The estimates of 0.1 mm to 0.2 mm for r_c yield a range for F_0 of $6 \leq F_0 \leq 24$.

In order to compare our conductivity measurements with percolation theory, we must exclude data below $\phi_c \approx 0.05$ [12], since the theory is only valid for $\phi > \phi_c$. It is more illustrative to display the data in terms of the reciprocal $G = 1/F = \rho_v^*/\rho_b$, which is the vertical resistivity formation factor. In Figure 2 e and f we show the two data sets from the Antarctic and Arctic. By fixing the exponent $t = 2$ and the threshold value $\phi_c = 0.05$ in the above expression for $F(\phi)$, a statistical best fit of the data yields a value of $F_0 \approx 9$, which lies inside our predicted range, so that

$$F(\phi) \sim 9 (\phi - 0.05)^2, \quad \phi \rightarrow \phi_c^+. \quad [4]$$

We see that the data agree well with the theory, and that they both exhibit divergent behavior with a vertical asymptote at the percolation threshold. Moreover, in the logarithmic variables $x = \log(\phi - 0.05)$ and $y = \log F$, the line predicted by percolation theory in (4) is $y = 2x + \log F_0$, with $\log F_0 = 0.95$, $F_0 = 9$. Critical path analysis yields the bounds $0.8 \leq \log F_0 \leq 1.4$, and the statistical best fit for the Antarctic data in f is $y = 1.99x + 0.93$, where 0.93 lies inside these bounds. In logarithmic variables, the standard error of the regression is 0.38 for the Arctic data and 0.22 for the Antarctic data (that is, approximately 68% of the Antarctic data is within 0.22 of the regression line). The increased scatter in the Arctic data is not surprising given the substantial inverse computation required to obtain the formation factor data.

To model $\sigma_v^*(\phi)$ over all porosities, we consider features of the brine phase present over the full range – some degree of small-scale connectivity, and self-similarity. Hierarchical models of spheres or other grains surrounded by smaller spheres, and so on, with brine in the pore spaces [12], were used to model $k_v^*(\phi)$. The simplest model yields a result of $k_v^*(\phi) = k_0 \phi^3$. Via (3) we obtain an Archie's law result of $F(\phi) = F_0 \phi^3$. A statistical best fit of our Antarctic data yields a value of $F_0 \approx 16$, which is in the estimated range. In Figure 3 a, our Antarctic data is shown along with fits derived from both models, and in b, Arctic permeability data [12] is shown relative to predictions from both models.

Figure 4 illustrates how we can derive information about the permeability structure and relevant transport processes from resistivity soundings of Arctic sea ice with *in situ* electrode strings [33]. Thus, the different formation factor regimes shown correspond to different permeability classes, with the lowermost ice layers permeable enough to allow for gas and nutrient exchange conducive to biomass build-up and CO₂ pumping [41], based on a critical permeability of 4×10^{-11} m², corresponding to a resistivity formation factor of 31.3 for $r_c = 0.1$ mm. This permeable base layer increases in vertical extent as the ice warms and thins due to bottom and surface melt. The ice interior is permeable enough to allow for meltwater flushing and reduction of ice salinity at surface ablation rates of 10 cm/d or less even prior to the onset of melt [42], corresponding to a resistivity formation factor of 625. High resistivity formation factors near the top in Figure 4 b are in part explained by such percolation of freshwater below accumulations of surface melt water.

It has been demonstrated in field experiments conducted in both the Arctic and Antarctic that sea ice exhibits critical behavior in its electrical transport properties at a percolation threshold. Such behavior provides the electrical signature of a key transition in fluid transport properties, known as the *rule of fives*, which determines whether or not fluid can flow through sea ice. This transition constrains a broad range of processes which are important in the geophysics and biology of the polar regions. The phenomenon is explained theoretically using percolation theory, which provides a universal power law describing the data from both poles, as well as a rigorous link between the fluid and electrical transport properties of sea ice. Our findings open the door to a new generation of techniques for *in situ* analysis and remote monitoring of transport processes which are critical to improving projections of the future trajectory of the polar ice packs.

Methods

Traditional surface-based geophysical techniques for *in situ* measurements, such as the Wenner array used for surface impedance tomography, have been used to study the resistivity profile of sea ice, particularly its anisotropic structure [24, 26, 27, 28, 29, 32]. During SIPEX we adapted the Wenner array to directly measure the vertical component of the anisotropic conductivity tensor σ^* of sea ice. At 8 of the 15 ice stations along the cruise track of the Australian icebreaker *Aurora Australis*, we extracted vertical cores from thin first-year sea ice, with lengths ranging from 34 cm to 86 cm. Thermistor probes were inserted into small holes drilled every 5 cm. We used a Wenner electrode array along sections of the cores, connected to a YEW Earth Resistance Tester operating at 38 Hz, as indicated in Figure 1 a and b. This set-up yields the resistance along the axis of the cylindrical ice core between probes P1 and P2, corresponding to the vertical direction *in situ*, with $a = L = 10$ cm (or $a = L = 5$ cm in some cases). After the temperature and resistance measurements were taken, which took about 10 to 20 minutes, we cut each core into 10 cm sections which were later melted, so that we could obtain bulk salinity measurements for each section. The temperature and salinity measurements allowed us to calculate a brine volume fraction profile for each core [43].

Plate electrodes in contact with the ends of a cylinder generate parallel field lines which make measuring the conductivity of the cylinder material relatively straightforward, as illustrated in Figure 5 a. To assess the accuracy of our four probe method, the commercial package Comsol 3.5a was used to create a finite element model of cylindrical sea ice

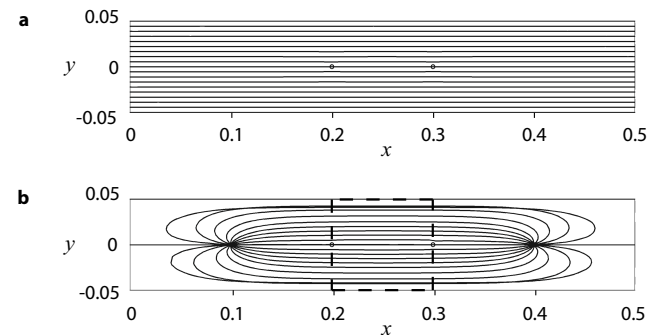


Fig. 5. Comparison of field lines for a parallel plate configuration in (a) with those for a four probe Wenner array in (b).

cores 0.09 m in diameter and 0.5 m in length. Four metal probes of 0.004 m in diameter and 0.09 m in length were inserted approximately 0.07 m into the core, similar to Figure 1 b. When the current is injected through the outer probes instead of parallel plates, as in Figure 5 b, the nearby field lines show significant curvature. However, in the boxed measurement region in Figure 5 b where the inner probes are located, the field lines are relatively straight, thus minimizing the error between the actual conductivity of the material and what is measured by the array. Numerical simulations show that if the outer probes are 5 cm or more from the inner measurement region, this error is less than 8.5%, and is less than 1.5% if the distance is 10 cm or more, as for much of our data.

When extracting a sea ice core to measure its properties, loss of brine is a principal concern. However, for our experiments we did not see any evidence of significant brine loss during the relatively short measurement periods with air temperatures ranging from about -6°C to -18°C (with most

below -9°C). Moreover, the probes are inserted deep into the core, minimizing contact with potential brine surface films. Our numerical simulations and these observations establish the Wenner array as a viable field method for *direct* resistivity measurements.

ACKNOWLEDGMENTS. We are grateful for the support provided by the Division of Mathematical Sciences (DMS), the Arctic Natural Sciences (ARC) Program, and the Office of Polar Programs (OPP) at the US National Science Foundation (NSF) through grants DMS-0537015, DMS-0940249, and ARC-0934721. Joyce Lin was supported by an NSF Postdoctoral Fellowship through a VIGRE grant (DMS-0602219) to the Department of Mathematics at the University of Utah. Adam Gully and Christian Sampson were partially supported by the NSF Research Experiences for Undergraduates (REU) Program through the VIGRE grant, and graduate support through VIGRE. This work was also supported in part by the Australian Government through the Antarctic Climate and Ecosystems Cooperative Research Centre. Finally, we thank the crew of the *Aurora Australis* for their help and support during the SIPEX Antarctic expedition.

1. Thomas, D. N. & Dieckmann, G. S. eds. (2009) *Sea Ice*, 2nd Edition. (Wiley-Blackwell, Oxford).
2. Serreze, M. C., Holland, M. M., & Stroeve, J. (2007) Perspectives on the Arctic's shrinking sea-ice cover. *Science* 315, 1533–1536.
3. Boé, J., Hall, A., & Qu, X. (2009) September sea-ice cover in the Arctic Ocean projected to vanish by 2100. *Nature Geoscience* 2, 341–343.
4. Fritsen, C. H., Lytle, V. I., Ackley, S. F., & Sullivan, C. W. (1994) Autumn bloom of Antarctic pack-ice algae. *Science* 266, 782–784.
5. Lizotte, M. P. & Arrigo, K. R. eds. (1998) *Antarctic Sea Ice: Biological processes, interactions and variability*. (American Geophysical Union, Washington D.C.).
6. Eicken, H. (1992) The role of sea ice in structuring Antarctic ecosystems. *Polar Biol.* 12, 3–13.
7. Krembs, C., Eicken, H., & Deming, J. W. (2011) Exopolymer alteration of physical properties of sea ice and implications for ice habitability and biogeochemistry in a warmer Arctic. *Proc. Natl. Acad. Sci.* 108, 3653–3658.
8. Perovich, D. K., Grenfell, T. C., Light, B., & Hobbs, P. V. (2002) Seasonal evolution of the albedo of multiyear Arctic sea ice. *J. Geophys. Res. (Oceans)* 107, 8044, doi:10.1029/2000JC000438.
9. Scott, F. & Feltham, D. L. (2010) A model of the three-dimensional evolution of Arctic melt ponds on first-year and multiyear sea ice. *J. Geophys. Res.* 115, C12064, doi:10.1029/2010JC006156.
10. Polashenski, C., Perovich, D., & Courville, Z. (2012) The mechanisms of sea ice melt pond formation and evolution. *J. Geophys. Res. C (Oceans)* 117, C01001 (23 pp.), doi:10.1029/2011JC007231.
11. Eicken, H., Grenfell, T. C., Perovich, D. K., Richter-Menge, J. A., & Frey, K. (2004) Hydraulic controls of summer Arctic pack ice albedo. *J. Geophys. Res. (Oceans)* 109, C08007.1–C08007.12.
12. Golden, K. M., Eicken, H., Heaton, A. L., Miner, J., Pringle, D., & Zhu, J. (2007) Thermal evolution of permeability and microstructure in sea ice. *Geophys. Res. Lett.* 34, L16501 (6 pages and issue cover), doi:10.1029/2007GL030447.
13. Perovich, D. K., Light, B., Eicken, H., Jones, K. F., Runciman, K., & Nghiem, S. V. (2007) Increasing solar heating of the Arctic Ocean and adjacent seas, 1979–2005: Attribution and role in the ice-albedo feedback. *Geophys. Res. Lett.* 34, L19505, doi:10.1029/2007GL031480.
14. Perovich, D. K., Richter-Menge, J. A., Jones, K. F., & Light, B. (2008) Sunlight, water, and ice: Extreme Arctic sea ice melt during the summer of 2007. *Geophys. Res. Lett.* 35, L11501, doi:10.1029/2008GL034007.
15. Eisenman, I. & Wettlaufer, J. S. (2009) Nonlinear threshold behavior during the loss of Arctic sea ice. *Proc. Natl. Acad. Sci.* 106, 28–32.
16. Notz, D. (2009) The future of ice sheets and sea ice: Between reversible retreat and unstoppable loss. *Proc. Natl. Acad. Sci.* 106, 20590–20595.
17. Flocco, D., Feltham, D. L., & Turner, A. K. (2010) Incorporation of a physically based melt pond scheme into the sea ice component of a climate model. *J. Geophys. Res.* 115, C08012 (14 pp.), doi:10.1029/2009JC005568.
18. Pedersen, C. A., Roeckner, E., Lüthje, M., & Winther, J. (2009) A new sea ice albedo scheme including melt ponds for ECHAM5 general circulation model. *J. Geophys. Res.* 114, D08101, doi:10.1029/2008JD010440.
19. Lytle, V. I. & Ackley, S. F. (1996) Heat flux through sea ice in the Western Weddell Sea: Convective and conductive transfer processes. *J. Geophys. Res.* 101, 8853–8868.
20. Rysgaard, S., Bendtsen, J., Pedersen, L. T., Ramløv, H., & Glud, R. N. (2009) Increased CO_2 uptake due to sea ice growth and decay in the Nordic Seas. *J. Geophys. Res.* 114, C09011, doi:10.1029/2008JC005088.
21. Maksym, T. & Markus, T. (2008) Antarctic sea ice thickness and snow-to-ice conversion from atmospheric reanalysis and passive microwave snow depth. *J. Geophys. Res.* 113, C02512, doi:10.1029/2006JC004085.
22. Golden, K. M., Ackley, S. F., & Lytle, V. I. (1998) The percolation phase transition in sea ice. *Science* 282, 2238–2241.
23. Pringle, D. J., Miner, J. E., Eicken, H., & Golden, K. M. (2009) Pore-space percolation in sea ice single crystals. *J. Geophys. Res. (Oceans)* 114, C12017, 12 pp., doi:10.1029/2008JC005145.
24. Fujino, K. & Suzuki, Y. (1963) An attempt to estimate the thickness of sea ice by electrical resistivity method ii. *Low Temp. Sci.* A21, 151–157.
25. Addison, J. (1969) Electrical properties of saline ice. *J. Appl. Phys.* 40, 3105–3114.
26. Thyssen, F., Kohnen, H., Cowan, M. V., & Timco, G. W. (1974) DC resistivity measurements on the sea ice near pond inlet. *Polarforschung* 44, 117–126.
27. Buckley, R. G., Staines, M. P., & Robinson, W. H. (1986) In situ measurements of the resistivity of Antarctic sea ice. *Cold Reg. Sci. Technol.* 12, 285–290.
28. Reid, J. E., Pfaffling, A., Worby, A. P., & Bishop, J. R. (2006) In situ measurements of the direct-current conductivity of Antarctic sea ice: Implications for airborne electromagnetic sounding of sea-ice thickness. *Ann. Glaciol.* 44, 217–223.
29. Ingham, M., Pringle, D. J., & Eicken, H. (2008) Cross-borehole resistivity tomography of sea ice. *Cold Reg. Sci. Technol.* 52, 263–277, 10.1016/j.coldregions.2007.05.002.
30. Wong, P. (1988) The statistical physics of sedimentary rocks. *Physics Today* 41, 24–32.
31. Haas, C. (2004) Late-summer sea ice thickness variability in the Arctic Transpolar Drift 1991–2001 derived from ground-based electromagnetic sounding. *Geophys. Res. Lett.* 31, L09402, doi:10.1029/2007GL030447.
32. Sampson, C., Golden, K. M., Gully, A., & Worby, A. P. (2011) Surface impedance tomography for Antarctic sea ice. *Deep Sea Res.* 58, 1149–1157.
33. Jones, K. A., Ingham, M., Pringle, D. J., & Eicken, H. (2010) Temporal variations in sea ice resistivity: resolving anisotropic microstructure through cross-borehole dc resistivity tomography. *J. Geophys. Res.* 115, C11023, doi:10.1029/2009JC006049.
34. Druckenmiller, M. L., Eicken, H., Johnson, M. A., Pringle, D. J., & Williams, C. C. (2009) Towards an integrated coastal sea-ice observatory: System components and a case study at Barrow, Alaska. *Cold Reg. Sci. Technol.* 56, 61–72.
35. Stauffer, D. & Aharony, A. (1992) *Introduction to Percolation Theory*, Second Edition. (Taylor and Francis Ltd., London).
36. Golden, K. (1990) Convexity and exponent inequalities for conduction near percolation. *Phys. Rev. Lett.* 65, 2923–2926.
37. Halperin, B. I., Feng, S., & Sen, P. N. (1985) Differences between lattice and continuum percolation transport exponents. *Phys. Rev. Lett.* 54, 2391–2394.
38. Berkowitz, B. & Balberg, I. (1992) Percolation approach to the problem of hydraulic conductivity in porous media. *Transport in Porous Media* 9, 275–286.
39. Friedman, A. P. & Seaton, N. A. (1998) Critical path analysis of the relationship between permeability and electrical conductivity of three-dimensional pore networks. *Water Resources Res.* 34, 1703–1710.
40. Stogryn, A. & Desargant, G. J. (1985) The dielectric properties of brine in sea ice at microwave frequencies. *IEEE Trans. Antennas Propagat.* AP-33, 523–532.
41. Rysgaard, S., Glud, R. N., Sejr, M. K., Bendtsen, J., & Christensen, P. B. (2007) Inorganic carbon transport during sea ice growth and decay: A carbon pump in polar seas. *J. Geophys. Res.* 112, C03016, doi:10.1029/2006JC003572.
42. Freitag, J. & Eicken, H. (2003) Meltwater circulation and permeability of Arctic summer sea ice derived from hydrological field experiments. *J. Glaciol.* 49, 349–358.
43. Eicken, H. (2003) in *Sea Ice: An Introduction to its Physics, Chemistry, Biology and Geology*, eds. Thomas, D. N. & Dieckmann, G. S. (Blackwell, Oxford), pp. 22–81.